Int. Journ. of Laser Science, Vol. 1, pp. 293–313
Reprints available directly from the publisher.
Photocopying permitted by license only.

Numerical Simulation of the Laser Welding of 2205 Duplex Stainless Steel

A. GHOSH[1,*], D. MISRA[1] AND S.K. ACHARYYA[2]

[1]*School of Laser Science & Engineering, Jadavpur University, Kolkata-700032, West Bengal, India*
[2]*Mechanical Engineering, Jadavpur University, Kolkata-700032, West Bengal, India*

Laser beam welding has become one of the promising welding techniques in diverse industries, such as aerospace, automotive, microelectronics, shipbuilding, *etc*., due to its superior features; namely, ease of automation, thin and small weld seams, minimum distortion and high welding speed. In this work the laser welding process is investigated considering phase change for butt joint welding of 2205 Duplex stainless steel plates *via* process modelling by finite element method (FEM) and statistical techniques. The objective of the present research is to investigate the effects of process parameters such as laser power, scanning speed and beam diameter on evolution of thermal field and formation of weld bead geometry. A three-dimensional (3-D) FEM numerical model with moving heat source is developed using COMSOL MULTIPHYSICS 4.2a. Statistical techniques are used to develop a mathematical model based on simulation results to predict maximum temperature and weld bead dimensions, namely, depth of penetration and bead width. Second order equations are developed by response surface methodology (RSM) to predict the responses, with significant accuracy. Effects of parameters and their interactions on the responses are studied, using the developed RSM models. Simulated results show that the maximum temperature at weld zone, bead width and depth of penetration increases with laser power and decreases with scanning speed. It is also seen that with increase of beam diameter, maximum temperature at weld zone and depth of penetration decreases while bead width increases. A multi-objective optimization on depth of penetration and bead width is conducted according to the desired optimisation criteria.

Keywords: 2205 Duplex stainless steel, laser welding, butt joint, bead width, depth of penetration, finite element method (FEM), response surface methodology (RSM)

*Corresponding author: E-mail: aritra.naihati@gmail.com

1 INTRODUCTION

Laser beam welding has been increasingly used for industrial manufacturing. The process of laser welding offers a great potential for new product design and development. The reasons for the increasing applications of laser welding over conventional techniques are some specific advantages of the process. Specifically, laser welding requires less amount of heat to be delivered to the workpiece resulting in a narrow heat affected zone (HAZ) and low distortion and effect on material properties [1].

A number of attempts have been made to simulate the laser welding process using numerical methods and experimental study with design of experiments (DOE) techniques. Frewin and Scott [2] presented a three-dimensional (3-D) finite element method (FEM) model of heat flow during pulsed laser beam welding. Their results suggest that temperature profile and weld dimensions are strong functions of absorptivity and energy distribution of the laser beam. De *et al.* [3] offered a two-dimensional (2-D) axisymmetric finite element analysis of heat flow during laser spot welding, taking into account the temperature dependence of physical properties and latent heat of transformations. They have suggested that using developed method, it has been possible to estimate the weld pool dimensions accurately. Benyounis and Olabi [4] furnished a comprehensive review on optimization techniques in order to obtain weld bead geometry. Ming *et al.* [5] dynamically simulated the temperature distribution in laser welding of 304 stainless steel. Anawa and Olabi [6] optimized the welding pool of dissimilar laser welded components using Taguchi method. Their results indicate that the developed models can predict the fusion zone and shape satisfactorily. Abderrazak *et al.* [7] utilized both techniques such as experimental and finite volume method to investigate the thermal phenomena during continuous laser keyhole welding. They have found that the shape and size of the molten pool in the workpiece are affected by welding parameters such as welding speed and laser power. Belhadj *et al.* [8] developed a 3-D FEM model to simulate thermal history of magnesium-based alloys during laser beam welding; moreover, they have conducted experimental studies to validate the results of numerical simulation and those are found to be in good agreement.

Abhilash and Sathiya [9] investigated the effect of the laser power, welding speed and focal point position on bead geometry. They have suggested that FEM can be used as a tool for predicting bead geometry at low values of heat input on laser welding. Shanmugam *et al.* [10] studied the effect of process parameters on weld bead geometry; that is, bead length, bead width and depth of penetration in laser spot welding of 2.5 mm thick AISI 304 stainless steel sheet. Their numerical simulation results predict the shape of weld beads for different ranges of laser input parameters and compared with experimental results which showed close agreement. Kumar *et al.* [11] performed a numerical investigation on transient temperature profile of laser beam weld-

ing process of titanium alloy considering combined double-ellipsoidal heat source model for both spot and moving heat source. They observed that peak temperature in the fusion zone increases with increased beam power; moreover, the size of the HAZ strongly depends on the power of the laser beam. Akbari *et al.* [12] compared numerical and experimental investigation of laser welding of titanium alloy for modelling of temperature distribution to predict the HAZ. They have found that for a lower welding speed, penetration depth increases at constant pulse duration, pulse frequency and power. Azizpour *et al.* [13] simulated laser welding process of Ti6Al4V 1.7 mm sheets in butt joint through finite element (FE) analysis to predict the temperature distribution, hardness and weld geometry. They observed that hardness at the centre of the weld pool is maximum and higher laser speeds caused more variation in hardness between the weld pool and base metal. Kumar [14] developed a 3-D FEM model using COMSOL MULTIPHYSICS for 2 mm thick AISI 316L stainless steel sheets by pulsed laser beam. They predicted the maximum/minimum temperature on AISI 316L stainless steel sheets during laser welding.

As can be seen from the literature review, not much work is reported on laser welding of 2205 Duplex stainless steels. Duplex stainless steel is used in diverse areas, such as, aerospace, marine, and fabrication industries. Duplex stainless steel represents a class of stainless steels with dual microstructure consisting of approximately equal proportions of ferrite and austenite phases. This balanced microstructure offers a favourable combination of mechanical strength and corrosion resistance and stability of mechanical and chemical properties at elevated temperatures. So, to discover the consequences of laser welding process on this combination steel, called Duplex, in this present work a 3-D numerical simulation using the FEM method is explored, which has been validated with published experimental work, to investigate the effects of process parameters on temperature profile and bead geometry formed due to laser welding of butt joint. In addition, the present work aims at developing correlations for prediction of maximum temperature at weld zone and weld bead geometry with varying laser process parameters (optimization using RSM based on FE simulated results instead of experimental results). COMSOL MULTIPHYSICS software is used for FE simulation.

2 FINITE ELEMENT (FE) SIMULATION

2.1 Model generation and assumptions

2205 Duplex stainless steel is used as the workpiece material. The dimension of the sample that is used for this study is shown in Figure 1(a). Due to the presence of symmetry in thermal loading and material geometry, only one half of the model is considered to reduce simulation time. This idealization of the model is adequate to represent the problem to achieve study goals [15].

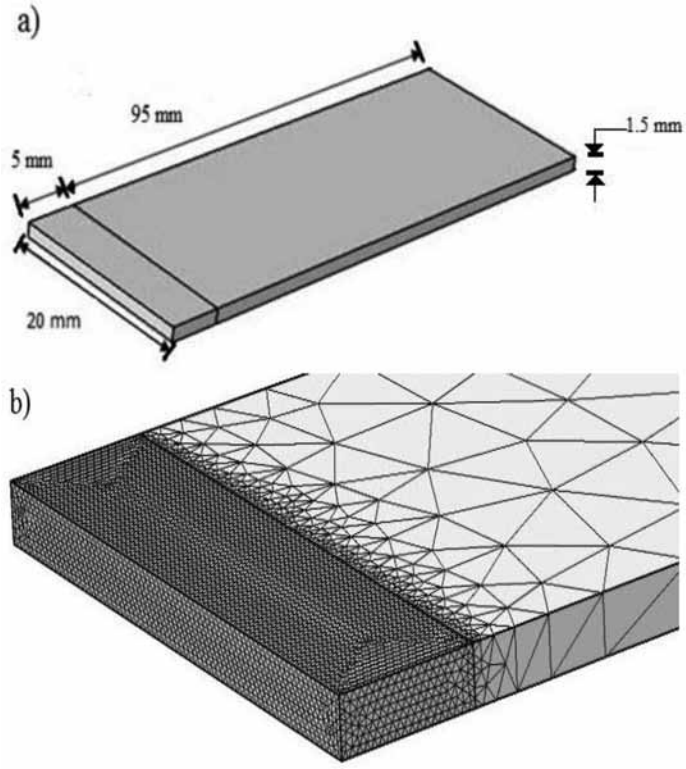

FIGURE 1
(a) One half of the symmetrical sample as *per* ASTM E8/E8M-09 and (b) FE mesh used for modelling.

Temperature dependent thermal properties are used, namely, thermal conductivity, specific heat and density and those are listed in Table 1 [16]. The initial temperature of workpiece is considered as 300 K. The laser beam is modelled as a moving volumetric heat source with small time increment. A 3-D free tetrahedral mesh with non-uniform mesh density is used to minimize the simulation time and memory requirement. Due to high heat flux involved along the laser path, very fine meshes are used along the path of the laser beam. Coarse meshes are used in other parts of the plate. Figure 1(b) shows the typical mesh used for FE simulation.

The transient temperature field developed during the laser welding process is assumed to follow Fourier's law of heat conduction. The following assumptions are made to develop a model for simulation of the laser welding process using FEM:

(i) Material properties of the workpiece are isotropic;
(ii) The distribution of laser intensity follows a Gaussian mode;

TABLE 1
Temperature dependent thermal properties of 2205 Duplex stainless steel [16].

Temperature (K)	Thermal Conductivity (W/mK)	Specific Heat (J/kgK)	Density (kg/m^3)
250	15	500	7860
500	18	500	
750	20	500	
1000	25	600	
1250	27.5	620	
1500	30	700	
1750	35	750	
1950	45	850	
2250	55	1000	
2500	65	1250	

(iii) Within the workpiece, heat transfer takes place by conduction, obeying Fourier's law and heat loss by combined free convection and radiation are considered from the surfaces of the sheet metal to the surrounding air; and
(iv) During the simulation process maximum surface temperature exceeds the liquidus temperature and hence the phase change has been considered.

2.2 Governing equation and boundary conditions

The following 3-D heat conduction equation is considered to model heat transfer in laser welding that defines the temperature distribution within the body.

$$\frac{\partial}{\partial x}\left(k(T)\frac{\partial T}{\partial x}\right)+\frac{\partial}{\partial y}\left(k(T)\frac{\partial T}{\partial y}\right)+\frac{\partial}{\partial z}\left(k(T)\frac{\partial T}{\partial z}\right)+Q_v=\rho(T)c_P(T)\left(\frac{\partial T}{\partial t}\right) \quad (1)$$

where $k(T)$ is the thermal conductivity as a function of temperature $\rho(T)$ is the density as a function of temperature, $c_p(T)$ is the specific heat as a function of temperature and Q_v is the volumetric heat flux.

In this work the laser beam is modelled through a volumetric Gaussian heat source, to simulate a realistic transfer of the energy to the workpiece. The heat source used in this present study can be expressed as [17, 18]

$$Q_v = Q(x,y,z) = \frac{3P(1-R)}{\pi abd}\exp\left(-\frac{3x^2}{a^2}\right)\exp\left(-\frac{3y^2}{b^2}\right)\exp\left(-\frac{3z^2}{d^2}\right) \quad (2)$$

where P is the power of the incident laser beam and R is the reflectivity. The parameters a, b are taken to be equal to the radius of the laser beam, d is the max depth. The material cooling phase is made through natural convection and radiation from its surfaces exposed to ambient air.

The convection boundary condition can be expressed as

$$q_{conv} = h(T_{st} - T_o) \quad (3)$$

where h is the heat transfer coefficient, which is taken as 10 W/m^{2}K [16]; T_{st} is the sheet metal surface temperature; and T_0 is the ambient temperature, which is taken as 300 K. The radiation boundary condition can be expressed as

$$q_{rad} = \varepsilon\sigma\,(T_{st}^{\,4} - T_o^{\,4}) \quad (4)$$

where ε is the emissivity, which is taken as 0.7 [16] and σ is the Stefan Boltzmann constant (5.6703×10^{-8} W/m^{2}K^4).

The temperature in the fusion zone reaches beyond the melting point of the material during the welding process. Therefore, a phase change phenomenon is incorporated in FE simulation by specific heat capacity method [19]:

$$c_p = c_{p,solid}\left(1-\alpha(T)\right) + c_{p,liquid}\left(\alpha(T)\right) + L_f\frac{\partial\alpha}{\partial T}) \quad (5)$$

$$\alpha(T) = \begin{Bmatrix} 1 & T \geq T_l \\ \dfrac{T-T_s}{T_l-T_s} & T_s \leq T \leq T_l \\ 0 & T \leq T_s \end{Bmatrix}$$

For the solid phase, $\alpha(T) = 0$, and for only liquid, $\alpha(T) = 1$. Latent heat of material is considered as $L_f = 500$ kJ/kg [16]. The material solidus (T_s) and liquidus (T_l) temperature are considered as 1658 and 1773 K, respectively [16].

2.3 Validation of the numerical model

The results are compared with published results of Shanmugam *et al*. [10] and Batahgy *et al*. [20], to validate the capability of the present numerical

TABLE 2
Validation of weld bead dimensions for laser power of 1000 W, scanning speed of 750 mm/min and plate thickness of 2.5 mm, with Shanmugam *et al*. [10].

Response Parameters	**From Simulation Study (f_t)**	**From Simulation and Experimental Study of Shanmugam *et al*.(f_s)**	**Percentage Error** $\left[\frac{f_t - f_s}{f_s} \times 100\right]$
Depth of penetration (mm)	1.99	1.98	0.51
Bead width (mm)	1.60	1.56	2.56
Peak temperature (°C)	3016	3025	–0.3

TABLE 3
Validation of weld bead dimensions for laser power of 8 kW, scanning speed of 0.5 m/min and plate thickness of 6.4 mm, with Batahgy *et al*. [20].

Response Parameters				
From simulation study			**From experimental study of Batahgy *et al.***	**Percentage error** $\left[\frac{f_t - f_s}{f_s} \times 100\right]$
Depth (mm)	**Width (mm)**	**Depth/Width ratio (f_t)**	**Depth/Width ratio (f_s)**	
5.15	5	1.03	0.99	4.04

model. Materials which were used for validation are AISI 304 stainless steel and 2205 Duplex stainless steel respectively. The plate size and process parameters are taken from their work for validation. The depth of penetration, bead width and maximum temperature obtained from the simulations are compared to the experimental results by Shanmugam *et al*. [10] and Batahgy *et al*. [20]. Table 2 and 3 summarizes the input parameters, the simulation results of maximum temperature and weld bead dimensions and percentages of error for validation cases. It is seen that the results of the present model are in good agreement with those of Shanmugam et al. [10] and Batahgy *et al*. [20].

3 TRANSIENT TEMPERATURE FIELD ANALYSIS

The transient temperature distribution obtained with the developed FEM model is presented for laser power of 500 W, scanning speed of 750 mm/min, spot diameter of 1 mm and plate thickness of 1.5 mm. Figure 2 shows the temperature distribution of the plate at four instances of time: (a) when the laser beam is at beginning of the plate (at $t = 0.1008$ seconds), (b) when the laser beam is

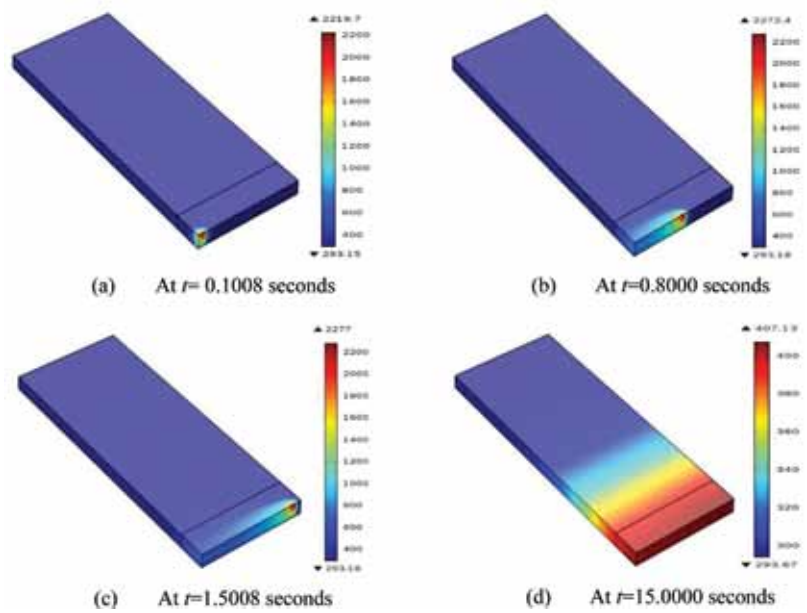

FIGURE 2
Temperature distribution at four instances when (a) the laser beam is at the beginning, (b) the laser beam is in the middle, (c) the laser beam is at the farthest edge and (d) after cooling for a laser power of 500 W, scanning speed of 750 mm/min, beam diameter of 1 mm and plate thickness of 1.5 mm.

at the centre of the plate (at $t = 0.8000$ seconds), (c) when the laser beam is at the farthest edge of the plate (at $t = 1.5008$ seconds) and (d) after 15.0000 seconds. During heating, peak temperature of 2277 K is reached at the farthest point on the weld line. After 15.0000 seconds the temperature drops further in the range of 300 to 407 K. The maximum temperature history along the scan line of the plate is shown in Figures 3(a) to (c) for different laser power, beam diameter and scanning speed while other process parameters are kept constant.

It can be seen from Figure 3 that maximum temperature starts increasing gradually on the top surface and attains a steady maximum in latter part of heating, barring the part near the farthest end. The maximum temperature increases further when laser beam reaches the upper edge of the plate. Figure 3(a) shows that with increase of power the maximum temperature increases as applied heat input to the material increases. It is evident from Figure 3(b) that with increase of scanning speed maximum temperature decreases. The reason behind this is higher scanning speed reduces the interaction time between applied heat source and material surface. In Figure 3(c), we see that with the increase of beam diameter maximum temperature decreases as higher beam diameter reduces the applied heat flux, resulting in decreased heat input *per* unit area to the material.

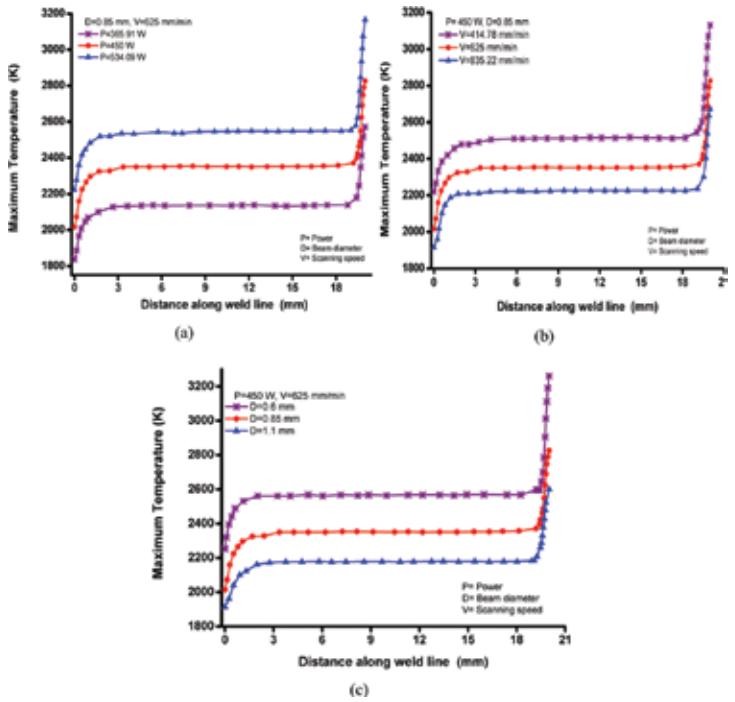

FIGURE 3
Maximum temperature at the top surface of the material with distance along the weld line for different (a) laser power, (b) scanning speed and (c) beam diameter.

We can see the temporal evolution of temperature at the midpoint (10 mm) along the weld line on the top surface of the plate from Figures 4(a) to (c) for different powers, scanning speeds and beam diameters. Figure 4(a) demonstrates that nodal temperature increases with increase in power as applied heat input to the material increases. It is clear from Figure 4(b) that with increase of scanning speed total time required for a simulation decreases and also nodal temperature decreases because higher scanning speed reduces the interaction time between applied heat source and material surface. It is observed from Figure 4(c) that with increase of beam diameter nodal temperature decreases as higher beam diameter reduces the applied heat flux, resulting in decreased heat input per unit area to the material.

4 DEVELOPMENT OF THE MATHEMATICAL MODEL

4.1 Response surface methodology (RSM)

RSM is a set of mathematical and statistical techniques that are useful for empirical model and optimization. A model predicting the response for some

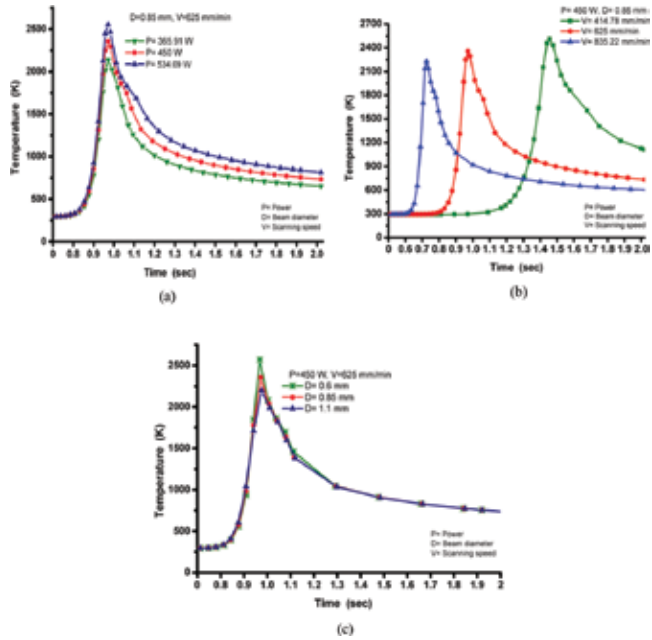

FIGURE 4(A- C)
Temporal variation of temperature for different (a) laser power, (b) beam diameter and (c) scanning speed on the upper surface of the plate at the midpoint (10 mm) of weld scan line.

independent input variables can be obtained by conducting experiments and applying regression analysis [21, 22]. If all variables are assumed to be measurable, the response surface can be expressed as

$$y = f(x_1, x_2, x_3, ...x_n) \pm \varepsilon \tag{7}$$

where y is the response, f is the function of response, ε is the experimental error, and $(x_1, x_2, x_3, ...x_n)$ are independent parameters. The application of RSM is to use a sequence of designed experiments to obtain an approximate relationship between a true response and the number of design variables, based on the observed data from the process or system. In the present work, response is collected from numerical simulation for laser welding of 2205 Duplex stainless steel.

4.2 Design matrix

The process parameters (low and high levels) and their notation and units are presented in Table 4. A central composite design matrix with three factors (laser power, scanning speed and laser beam diameter) and five levels ($-\alpha$, -1, 0, $+1$, $+\alpha$), is considered. The RSM is applied to create the design matrix for attaining the regression equations and to generate the statistical response

TABLE 4
Process parameters and their units and limits.

Parameter	Notation	Unit	Low Actual	High Actual
Laser power	P	W	400	500
Scanning speed	V	mm/min	500	750
Beam diameter	D	mm	0.7	1.0

plots. The numerical simulations are carried out according to the design matrix and the maximum temperature and weld bead dimensions as responses are listed in Table 5. The adequacy of the models is tested using the sequential *f*-test and the analysis of variance (ANOVA) technique using Design Expert® 7.0 software to attain the best-fit models.

4.3 Analysis of variance (ANOVA)

ANOVA is used to separate the total variation in a set of data into two or more components. The source of variation is identified so that one can see its influence on the total variation. It is also used to compare means where there are three or more. ANOVA is used to analyse the data from experiments. The purposes are for estimating and testing hypotheses about population variances and population means:

$$H_0\text{: all means are equal: } \mu_1 = \mu_2 = \ldots \mu_{\mathrm{T.}}$$
$$H_A\text{: not all means are equal: } \mu_{\mathrm{i}} \neq \mu_{\mathrm{j.}}$$

The ANOVA test statistic is the variance ratio, which is distributed as F with the appropriate number of numerator degrees of freedom and denominator degrees of freedom at the chosen a level.

$$F = \frac{\textit{Among}\ \text{groups mean square}}{\textit{Within}\ \text{groups mean square}} = \frac{MS_{Group}}{MS_{Error}}$$

A large value of F means to reject the null hypothesis. A small value means not to reject. The ANOVA table has columns for degrees of freedom (*df*), sums of squares (SS), mean squares (MS). Total $df = \mathrm{N} - 1$ (N, the total number of observations), Group $df = \mathrm{k} - 1$ (k, the total number of groups), Error $df = \mathrm{N} - \mathrm{k}$. The error term reflects how much each individual measurement differs from the population mean of its group. Sum of Squares Total value (SS_{Total}) is the total variation in the data. SS_{Group} is the deviation of the estimated factor level mean around the overall mean. SS_{Error} is the deviation of an observation from its corresponding factor level mean:

TABLE 5
Design matrix and numerically calculated responses.

Sample No.	Process Parameters			Responses		
	Power (W)	Speed (mm/min)	Beam diameter (mm)	Maximum temperature (K)	Bead width (mm)	Depth of penetration (mm)
1	400.00	750.00	1.00	2052.99	0.53	0.60
2	450.00	625.00	0.85	2357.70	0.66	0.83
3	400.00	500.00	0.70	2434.31	0.66	0.97
4	400.00	500.00	1.00	2218.82	0.71	0.79
5	534.09	625.00	0.85	2553.91	0.75	1.17
6	450.00	835.22	0.85	2226.61	0.55	0.71
7	500.00	500.00	0.70	2691.40	0.81	1.22
8	400.00	750.00	0.70	2263.75	0.50	0.74
9	450.00	625.00	0.85	2357.70	0.66	0.83
10	450.00	625.00	0.85	2357.70	0.66	0.83
11	500.00	750.00	0.70	2525.60	0.65	1.00
12	365.91	625.00	0.85	2138.94	0.50	0.67
13	450.00	414.78	0.85	2517.81	0.85	1.06
14	450.00	625.00	0.85	2357.70	0.66	0.83
15	500.00	750.00	1.00	2279.20	0.61	0.80
16	500.00	500.00	1.00	2458.64	0.85	1.00
17	450.00	625.00	1.10	2179.77	0.68	0.74
18	450.00	625.00	0.85	2357.70	0.66	0.83
19	450.00	625.00	0.60	2569.81	0.61	0.96
20	450.00	625.00	0.85	2357.70	0.66	0.83

$$SS_{Total} = SS_{Group} + SS_{Error}$$

$$SS_{Group} = \sum n_i (\overline{y_i} - \overline{y})^2$$

$$SS_{Error} = \sum_i \sum_j (y_{ij} - \overline{y_i})^2$$

$$SS_{Total} = \sum_i \sum_j (y_{ij} - \overline{y_i})^2$$

$$MS_{Total} = MS_{Group} + MS_{Error}$$

$$\left.\begin{aligned} MS_{Error} &= \frac{SS_{Error}}{df_{Error}} \\ MS_{Group} &= \frac{SS_{Group}}{df_{Group}} \end{aligned}\right\}$$

$\overline{y_i}$ = Mean of the observations at i th level of group

$\overline{y}$ = Mean of all observations

y_{ij} = Value of the j th observations at i th level of group

4.4 Analysis of maximum temperature at the weld zone

The model F-value of 7145.64 implies the model is significant. There is only a 0.01% chance that a 'model F-value' this large could occur due to noise. The ANOVA table of the quadratic model with other adequacy measures R^2, adjusted R^2 and predicted R^2 are listed in Table 6. The adequacy measures R^2, adjusted R^2 and predicted R^2 are in reasonable agreement and are close to 1, which is representing that this regression model has greater predictive capability. The associated p-value of less than 0.05 for the model indicates model terms are significant. The adequate precision compares the signal to noise ratio and a ratio greater than 4 is desirable. The ANOVA results show that the effects of laser power (P), scanning speed (V) and beam diameter (D), the quadratic effect of the square of laser power (P^2), scanning speed (V^2) and beam diameter (D^2), and the two level interaction of laser power and beam diameter ($P\times D$) are the most significant model terms associated with the maximum temperature of the plate. The other model terms are not significant.

The final mathematical model for maximum temperature (T_M) in terms of actual factors as determined by Design-Expert® 7.0 software is

TABLE 6
ANOVA for response surface quadratic model of maximum temperature.

Source	Sum of Squares	Degree of Freedom	Mean Square	F-value	Prob>F, p-value
Model	4.879E+005	9	54215.55	7145.64	<0.0001
P	2.074E+005	1	2.074E+005	27331.57	<0.0001
V	1.005E+005	1	1.005E+005	13242.07	<0.0001
D	1.785E+005	1	1.785E+005	23527.94	<0.0001
PV	9.79	1	9.79	1.29	0.2825
PD	349.93	1	349.93	46.12	<0.0001
VD	9.92	1	9.92	1.31	0.2794
P^2	212.32	1	212.32	27.98	0.0004
V^2	401.63	1	401.63	52.94	<0.0001
D^2	552.29	1	552.29	72.79	<0.0001
Residual	75.87	10	7.59		
Lack of Fit	75.87	5	15.17		
Pure Error	0.000	5	0.000		
Corr. Total	4.880E+005	19			

Standard deviation=2.75	R^2=0.9998
Mean=2362.89	Adjusted R^2=0.9997
Coefficient of variation(%)=0.12	Predicted R^2=0.9987
Predicted residual error of sum of squares (PRESS)=642.66	Adequate precision=332.005

$$T_M = 1926.60170 + 4.70647 \times P - 0.97836 \times V - 795.97907 \times D - 1.77000 \times 10^{-4} \times P \times V - 0.88183 \times P \times D - 0.059400 \times V \times D - 1.53532 \times 10^{-3} \times P^2 + 3.37864 \times 10^{-4} \times V^2 + 275.13713 \times D^2 \quad (8)$$

4.5 Analysis of bead width

The model F-value of 151.06 implies the model is significant. There is only a 0.01% chance that a 'model F-value' this large could occur due to noise. The ANOVA table of the quadratic model with other adequacy measures R^2, adjusted R^2 and predicted R^2 are listed in Table 7. The adequacy measures R^2, adjusted R^2 and predicted R^2 are in reasonable agreement and are close to 1. The associated p-value of less than 0.05 for the model indicates model terms are significant. The adequate precision compares the signal to noise ratio and a ratio greater than 4 is desirable. The ANOVA results show that

TABLE 7
ANOVA for response surface quadratic model of bead width.

Source	Sum of Squares	Degree of Freedom	Mean Square	F-Value	Prob>F, p-value
Model	0.19	9	0.021	151.06	<0.0001
P	0.065	1	0.065	464.42	<0.0001
V	0.11	1	0.11	813.32	<0.0001
D	2.863E-003	1	2.863E-003	20.53	0.0011
PV	4.500E-004	1	4.500E-004	3.23	0.1027
PD	8.000E-004	1	8.000E-004	5.74	0.0376
VD	1.250E-003	1	1.250E-003	8.96	0.0135
P^2	1.611E-003	1	1.611E-003	11.55	0.0068
V^2	3.663E-003	1	3.663E-003	26.27	0.0004
D^2	1.768E-004	1	1.768E-004	1.27	0.2865
Residual	1.394E-003	10	1.394E-004		
Lack of Fit	1.394E-003	5	2.789E-004		
Pure Error	0.000	5	0.000		
Cor Total	0.19	19			

Standard deviation=0.012	R^2=0.9927
Mean=0.66	A djusted R^2=0.9861
Coefficient of variation(%)=1.79	Predicted R^2=0.9409
Predicted residual error of sum of squares (PRESS) = 0.011	Adequate precision=43.228

the effect of laser power (P), scanning speed (V) and beam diameter (D), the quadratic effects of the square of laser power (P^2) and scanning speed (V^2), and the two level interaction of laser power and beam diameter ($P \times D$) and scanning speed and beam diameter ($V \times D$) are the most significant model terms associated with the bead width. The other model terms are not significant.

The final mathematical model for bead width (B_W) in terms of actual factors as determined by Design-Expert® 7.0 software is

$$\begin{aligned} B_W = & -1.35840 + 7.06693 \times 10^{-3} \times P - 8.97834 \times 10^{-4} \\ & \times V + 1.37779 \times D - 1.20000 \times 10^{-6} \times P \times V \\ & -1.33333 \times 10^{-3} \times P \times D - 6.66667 \times 10^{-4} \\ & \times V \times D - 4.22927 \times 10^{-6} \times P^2 + 1.02037 \\ & \times 10^{-6} \times V^2 - 0.15565 \times D^2 \end{aligned} \tag{9}$$

4.6 Analysis of depth of penetration

The model F-value of 86.70 implies the model is significant. There is only a 0.01% chance that a 'model F-value' this large could occur due to noise. The ANOVA table of the quadratic model with other adequacy measures R^2, adjusted R^2 and predicted R^2 are listed in Table 8. The adequacy measures R^2, adjusted R^2 and predicted R^2 are in reasonable agreement and are close to 1. The associated p-value of less than 0.05 for the model indicates model terms are significant. The adequate precision compares the signal to noise ratio and a ratio greater than 4 is desirable. The ANOVA results show that the effects of laser power (P), scanning speed (V) and beam diameter (D), the quadratic effect of the square of laser power (P^2) and scanning speed (V^2) are the most significant model terms associated with the bead width. The other model terms are not significant.

The final mathematical model for depth of penetration (D_P) in terms of actual factors as determined by Design-Expert® 7.0 software is

$$\begin{aligned} D_P = & 3.56720 - 7.58608 \times 10^{-3} \times P - 2.76059 \times 10^{-3} \times V \\ & -0.60263 \times D + 0.000000 \times P \times V - 1.66667 \times 10^{-3} \\ & \times P \times D + 4.00000 \times 10^{-4} \times V \times D + 1.28684 \\ & \times 10^{-5} \times P^2 + 1.26698 \times 10^{-6} \times V^2 + 0.32987 \times D^2 \end{aligned} \tag{10}$$

TABLE 8
ANOVA for response surface quadratic model of depth of penetration.

Source	Sum of Squares	Degree of Freedom	Mean Square	F-Value	Prob>F, p-value
Model	0.49	9	0.054	86.70	<0.0001
P	0.23	1	0.23	363.47	<0.0001
V	0.15	1	0.15	239.24	<0.0001
D	0.090	1	0.090	144.43	<0.0001
PV	0.000	1	0.000	0.000	1.0000
PD	1.250E-003	1	1.250E-003	2.00	0.1876
VD	4.500E-004	1	4.500E-004	0.72	0.4159
P^2	0.015	1	0.015	23.88	0.0006
V^2	5.648E-003	1	5.648E-003	9.04	0.0132
D^2	7.939E-004	1	7.939E-004	1.27	0.2859
Residual	6.247E-003	10	6.247E-004		
Lack of Fit	6.247E-003	5	1.249E-003		
Pure Error	0.000	5	0.000		
Cor Total	0.49	19			

Standard deviation=0.025	R^2=0.9873
Mean=0.87	Adjusted R^2=0.9760
Coefficient of variation(%)=2.87	Predicted R^2=0.9037
Predicted residual error of sum of squares (PRESS) = 0.048	Adequate precision=35.628

5 EFFECTS OF PROCESS PARAMETERS ON THE RESPONSES

5.1 Maximum temperature at the weld zone

The effects of parameters on the response are identified through the developed RSM model. Figures 5(a) to (c) shows the 3-D surface plot of the effect of the interaction between process variables on the maximum temperature at weld zone. It is observed from these figures that the maximum temperature at weld zone increases when the laser power increases and decreases when scanning speed and beam diameter increases.

High power laser beam can deliver more power. Therefore, maximum temperature at weld zone increases with laser power. As scanning speed increases, interaction time between the workpiece and the laser beam decreases, resulting in reduced absorption of heat by the workpiece. Thus, the rate of temperature rise decreases with increase in scanning speed. It is also observed that maximum temperature at weld zone decreases with the increase in beam diameter because the power density per area decreases when beam diameter increases.

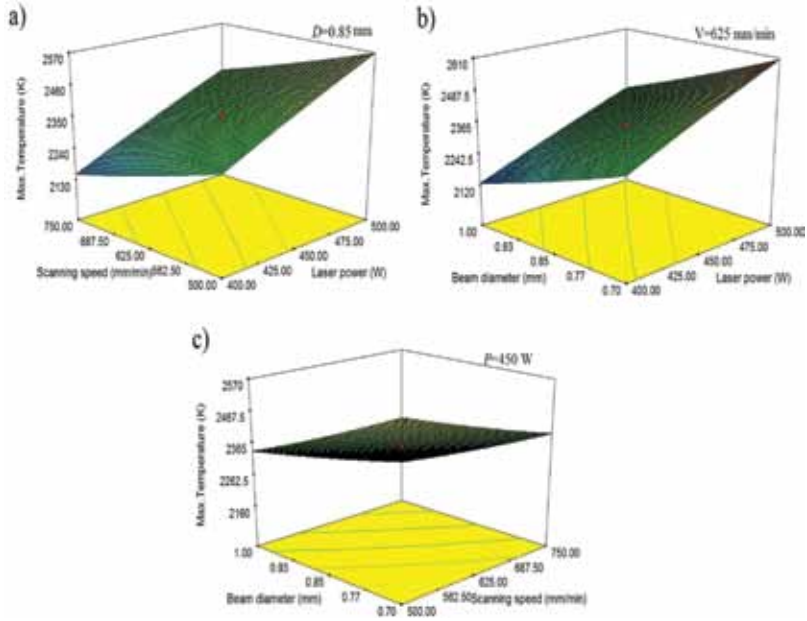

FIGURE 5
3-D plots showing the effect of input parameters on the maximum temperature at the weld zone.

5.2 Bead width

Figures 6(a) to (c) shows the 3-D surface plot of the effect of the interaction between process variables on bead width. It is seen from these figures that bead width increases when laser power and beam diameter increases and decreases when scanning speed increases. If power is increased, the workpiece absorbs more heat and resulting in increased bead width. Bead width decreases with scanning speed due to less heat absorption by workpiece because of reduced interaction time between the heat source and the workpiece. Bead width also increases with increase in beam diameter as beam diameter increases; the heat distribution takes place over a wider area, resulting in a wider bead width.

5.3 Depth of penetration

Figures 7(a) to (c) shows the 3-D surface plot of the effect of the interaction between process variables on depth of penetration. From these figures we can see that depth of penetration increases when laser power increases and decreases when scanning speed and beam diameter increases. When power increases, heat intake by the workpiece increases, results more heat penetration. With increase of scanning speed, interaction time of laser beam with

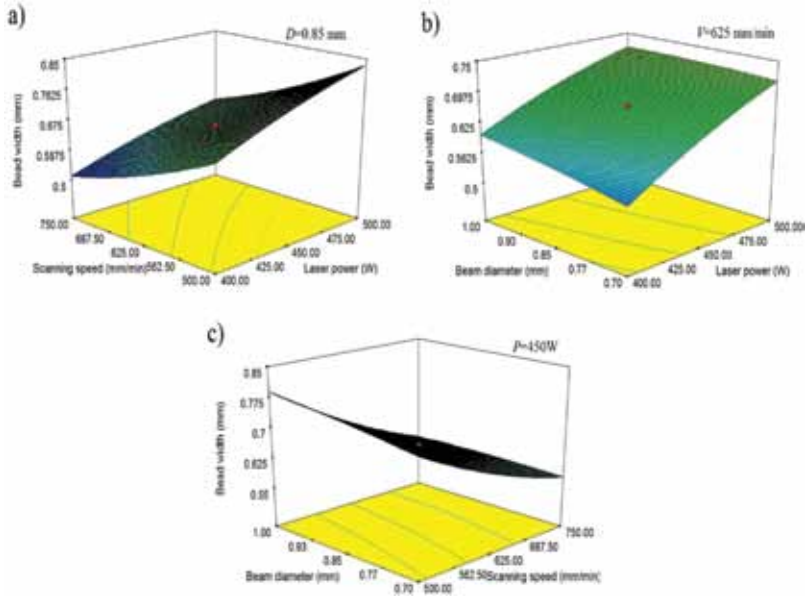

FIGURE 6
3-D plots showing the effect of input parameters on the bead width.

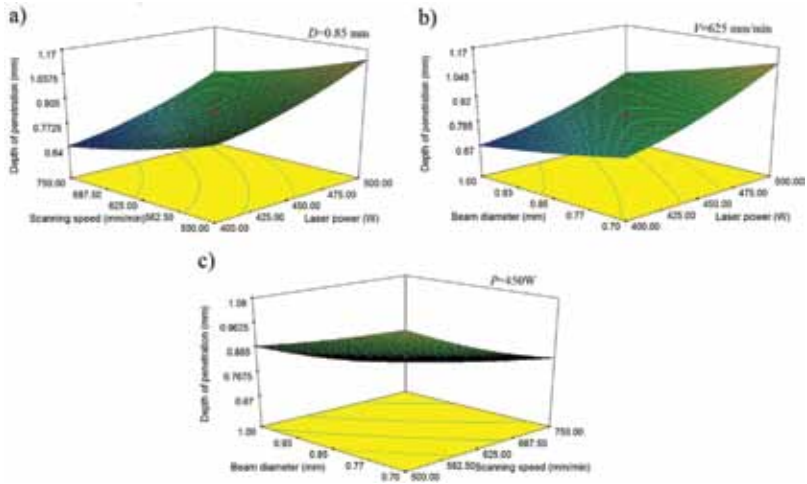

FIGURE 7
3-D plots showing the effect of input parameters on the depth of penetration.

workpiece decreases leading to less heat penetration into workpiece. As the power density per area decreases with increase of beam diameter less heat will be penetrated into the workpiece.

6 OPTIMIZATION

The aim of numerical optimization method, using Design Expert® 7.0 software, is to achieve a minimum bead width with maximum depth of penetration at relatively low-operating cost by using minimum laser power and maximum welding speed within the design space. Table 9 summarizes the goal, lower and upper limits and importance of each response which are derived from RSM.

Table 10 presents the best welding parameter combinations based on the criteria, stated in Table 9, which leads to achieve a minimum bead width with maximum depth of penetration at relatively low-operating cost by using minimum laser power and maximum welding speed within the design space. To achieve a near minimum bead width with near maximum depth of penetration, the optimum range of laser process parameters to be maintained are: laser power 400.00 to 424.95 W, scanning speed 747.80 to 695.37 mm/min and spot diameter 0.70 to 1.00 mm.

TABLE 9
The criteria of numerical optimization.

Parameter	Goal	Lower Limit	Upper Limit	Lower Weight	Upper Weight	Importance
P (W)	Minimize	400	500	1	1	3
V (mm/min)	Maximize	500	750	1	1	3
D (mm)	is in range	0.7	1.0	1	1	3
T_M (K)	is in range	2052.99	2691.40	1	1	3
B_W (mm)	Minimize	0.5	0.85	1	1	5
D_P (mm)	Maximize	0.6	1.22	1	1	5

TABLE 10
Optimal welding condition based on the criterion.

Sample No.	P (W)	V (mm/min)	D (mm)	B_W (mm)	D_P (mm)	T_M (K)	Desirability
1	400.00	683.82	0.70	0.522368	0.761008	2306.37	0.607 (Selected)
2	400.00	684.87	0.70	0.521899	0.760225	2305.72	0.607
3	400.00	695.37	0.70	0.517316	0.752536	2299.15	0.606
4	400.00	680.97	0.70	0.523766	0.762825	2307.68	0.606
5	400.00	687.26	0.70	0.520957	0.758072	2303.64	0.606
6	424.95	747.80	0.70	0.541412	0.764827	2334.65	0.601

7 CONCLUSIONS

Laser welding of 2205 Duplex stainless steel plate is simulated using a three-dimensional (3-D) finite element method (FEM) model and compared with available experimental results. The effects of process parameters on the temperature field and weld bead dimensions are studied and also compared with experimental results from published papers [10, 20]. Statistical techniques are used to develop mathematical models based on FEM simulation results to predict maximum temperature and weld bead dimensions. A multi-objective optimization on weld bead dimensions is conducted according to the desired optimization criteria. The following conclusions can be drawn from above investigations:

(i) Maximum temperature at weld zone increases with laser power and decreases with increase of scanning speed and spot diameter;
(ii) Bead width increases with laser power and spot diameter and decreases with increase in scanning speed;
(iii) Depth of penetration increases with laser power and decreases with increase in scanning speed and spot diameter; and
(iv) The optimum process parameters for minimum bead width with maximum depth of penetration at relatively low operating (energy) cost and high productivity are also found based on desirability function.

ACKNOWLEDGMENT

Aritra Ghosh expresses gratitude for the grants received for her Research Fellowship under TEQIP-COE Phase II of Jadavpur University.

REFERENCES

[1] Sathiya P., Abdul Jaleel M.Y., Katherasan D. and Shanmugarajan B. Optimization of laser butt welding parameters with multiple performance characteristics. *Optics & Laser Technology* **43**(3) (2011), 660–673.
[2] Frewin M. and Scott D. Finite element model of pulsed laser welding. *Welding Research Supplement* (1999), 15–22.
[3] De A., Maiti S., Walsh C. and Bhadeshia H. Finite element simulation of laser spot welding. *Science and Technology of Welding and Joining* **8**(5) (2003), 377–384.
[4] Benyounis K. and Olabi A. Optimization of different welding processes using statistical and numerical approaches – A reference guide. *Advances in Engineering Software* **39**(6) (2008), 483–496.
[5] Ming H.G., Jian Z. and Qang L.J. Dynamic simulation of the temperature field of stainless steel laser welding. *Materials & Design* **28**(1) (2007), 240–245.

[6] Anawa E.M. and Olabi A.G. Using Taguchi method to optimize welding pool of dissimilar laser-welded components. *Optics & Laser Technology* **40**(2) (2008), 379–388.

[7] Abderrazak K., Bannour S., Mhiri H., Lepalec G. and Autric M. Numerical and experimental study of molten pool formation during continuous laser welding of AZ91 magnesium alloy. *Computational Materials Science* **44**(3) (2009), 858–866.

[8] Belhadja A., Bessroura J., Masseb J.E., Bouhafsa M. and Barrallier L. Finite element simulation of magnesium alloys laser beam welding. *Journal of Materials Processing Technology* **210**(9) (2010), 1131–1137.

[9] Abhilash A.P. and Sathiya P. Finite element simulation of laser welding of 904L super austenitic stainless steel, *Transactions of the Indian Institute of Metals* **64**(4-5) (2011), 409–416.

[10] Shanmugam N.S., Buvanashekaran G. and Sankaranarayanasamy K. Some studies on weld bead geometries for laser spot welding process using finite element analysis. *Materials & Design* **34** (2012), 412–426.

[11] Kumar C., Das M. and Biswas P. A 3-D finite element analysis of transient temperature profile of laser welded Ti-6Al-4V alloy. *5th International & 26th All India Manufacturing Technology, Design and Research Conference (AIMTDR 2014)*. 12-14 December 2014, Guwahati, Assam, India.

[12] Akbari M., Saedodin S., Toghraie D., Razavi R.S. and Kowsari F. Experimental and numerical investigation of temperature distribution and melt pool geometry during pulsed laser welding of Ti6Al4V alloy. *Optics & Laser Technology* **59** (2014), 52–59.

[13] Azizpour M., Ghoreishi M. and Khorram A. Numerical simulation of laser beam welding of Ti6Al4V sheet. *Journal of Computational and Applied Research* **4**(2) (2015), 145-154.

[14] Kumar S. Numerical modeling and simulation of a butt joint welding of AISI 316L stainless steels using a pulsed laser beam. *Materials Today: Proceedings* **2**(4-5) (2015), 2256–2266.

[15] Acherjee B., Kuar A.S., Mitra S. and Misra D. Effect of carbon black on temperature field and weld profile during laser transmission welding of polymers: An FEM study. *Optics & Laser Technology* **44**(3) (2012), 514–521.

[16] Daha M.A., Nassef G.A., Abdallah I.A. and Abou Seeda H.M. Three-dimensional thermal finite element modeling for keyhole plasma arc welding of 2205 Duplex stainless steel plates. *International Journal of Engineering and Technology* **2** (2012), 2049-3444.

[17] Daneshkhah R., Najafi M. and Torabian H. Numerical simulation of weld pool shape during laser beam welding. *International Research Journal of Applied and Basic Sciences* **3**(8) (2012), 1624-1630.

[18] Marimuthu S., Eghlio R.M., Pinkerton A.J. and Li L. Coupled computational fluid dynamic and finite element multiphase modeling of laser weld bead geometry formation and joint strengths. *Journal of Manufacturing Science and Engineering* **135** (2013), 011004-1.

[19] Bannach N. (2014) *Phase Change: Cooling and Solidification of Metal*. Retrieved 12th June 2018, from https://uk.comsol.com/blogs/phase-change-cooling-solidification-metal/

[20] Batahgy A.M., Khourshid A.F. and Sharef T. Effect of laser beam welding parameters on microstructure and properties of Duplex stainless steel. *Materials Sciences and Applications* **2**(10) (2011), 1443-1451.

[21] Acherjee B, Kuar A., Mitra S. and Misra D. Modeling of laser transmission contour welding process using FEA and DoE. *Optics & Laser Technology*. **44**(5) (2012), 1281–1289.

[22] Montgomery D.C. *Design and Analysis of Experiments*. New York: Wiley. 2001.